3D Terahertz Antenna Measurement: A Comparison Between Solid-State Electronics and Photomixing Approaches

Jiexin Lai and Yang Yang

The terahertz spectrum (0.1–10 THz) is located between the infrared and microwave regimes, known as the Terahertz Gap. During the last decade, terahertz (THz) wave generation, detection and manipulation (three key THz research directions) have been significantly advanced, taking advantage of the rapid development of solid-state circuits and photonics technologies. Terahertz sources are critical in terahertz antenna measurement systems. There are two approaches for terahertz wave generation. The first approach is based on solid-state electronics to reach the terahertz regime, using microwave multiplexing techniques, which has a vector network analyzer (VNA) architect integrated with frequency extenders, a signal generator and a signal analyzer. The second approach is based on the photomixing technique to down-convert the laser beams using electro-optic (EO) crystal. The typical devices used by this approach include the THz time-domain spectroscopy (TDS), the photomixer, and the photoconductive antenna (PCA). Therefore, the terahertz antenna measurement systems can be categorized into two groups: (1) Solide-state electronics-based measurement and (2) Photonic-based measurement. This paper compares the state-of-the-art 3D terahertz antenna measurement platforms and their operation principles.

1. Solid-State Electronics-Based Measurement

The conventional diagram of the solid-state electronics-based measurement (SSEBM) system for antenna measurement is shown in Fig. 1. The antenna measurement setup is composed of a transmitting (Tx) and a receiving (Rx) device. They can be divided into direct far-field (DFF), indirect far-field (IFF), near-field (NF), and midfield measurement setups [1], which are subjected to the distance setup between the Tx side and the Rx side. The antenna under test (AUT) is connected to the Tx module on the Tx side. The TxRx module can realize transmitting and receiving for vector network analyzer (VNA) measurement. The key parameters of the AUT to be measured include the return loss $|S_{11}|$, the gain, the half-power beamwidth (HPBW), the sidelobe level (SLL), and the cross-polarization level (X-pol). Because of the complicated setup of the THz beam measurement platform, for example, the THz frequency extender configuration, the THz antenna's front-to-back ratio (FBR) is rarely measured. The VNA can measure the return loss $|S_{11}|$, while the gain of the AUT needs to be calculated by comparing the measured data with the gain of a standard horn antenna. The generator-analyzer measurement approach cannot measure the $|S_{11}|$.

Because of the higher atmospheric absorption of THz waves, the THz measurement system sometimes does not have to be in an anechoic chamber for the antenna main beam measurement. However, the anechoic chamber, positioning systems, and data processing algorithms are essential for high-precision measurement.

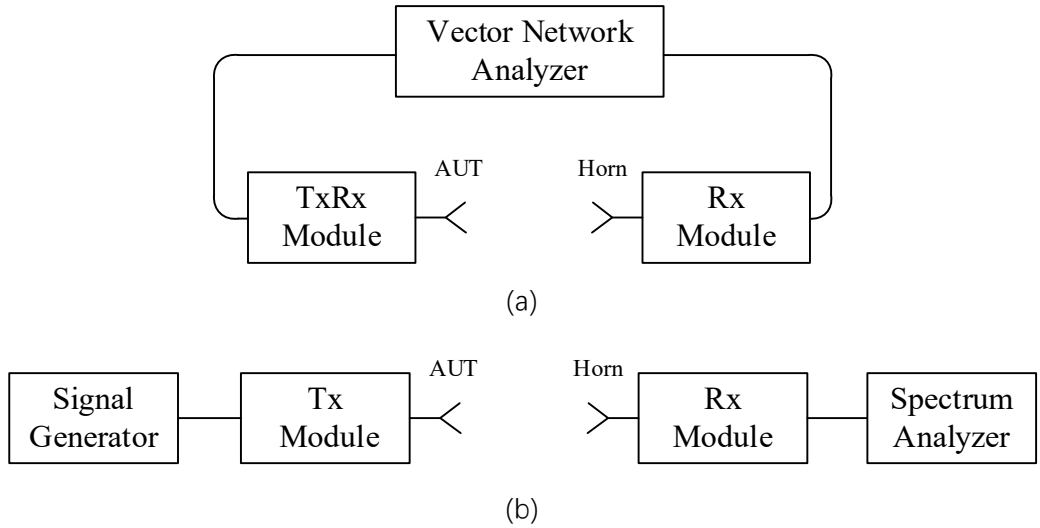

Fig. 1. The basic schematic diagram of the SSEBM systems: (a) VNA measurement. (b) Spectrum analyzer measurement

VNAs are the most common measurement devices in modern microwave laboratories. The first network analyzer for S-parameter measurement was proposed in the early 1950s [2], and it can only measure the S-parameters. As time passes, phase noise, amplitude-modulation (AM) noise, residual noise measurements, and nonlinear measurements are realizable by the VNA platform. In 1999, the two-port VNA up to 220 GHz was first proposed for the on-wafer measurement [3]. In 2005, VNA was proposed in the 220-325 GHz band [4].

In 2008, the two-port VNA from 325 to 508 GHz [5] was presented, which consists of an Agilent 50-GHz VNA and Oleson Microwave Laboratories (OML) WR 2.2 frequency extenders. By employing the line-reflect-line (LRL) calibration, the setup can measure the return losses ($|S_{11}|$, $|S_{22}|$) and the insertion losses ($|S_{21}|$, $|S_{12}|$) with dynamic ranges of better than 20 and 35 dB. In 2011, the VNA frequency extender reached 1.1 THz using WR 1.0 extenders [6] with a typical dynamic range of 70 dB. At present, the highest frequency of THz waves generated by solid-state electronics is 1.5 THz, which was proposed by Virginia Diodes, Inc. (VDI) [7].

The Tx and Rx modules are normally frequency extenders. The frequency extenders consist of a group of key components: isolators, amplifiers, doublers/multipliers, and harmonic mixers. The frequency mixer is an essential device in frequency upconversion and downconversion, which has two input ports and one output port. For the upconversion, the two input ports are known as the intermediate-frequency (IF) and local-oscillator (LO) ports, while the output port is the radio-frequency (RF) port. An ideal RF signal consists of the sum and difference frequencies of IF and LO signals. The RF signals are input into a mixer with the LO signals for downconversion. The frequency of the output IF signal is equal to the difference between the frequency of the RF and LO signals, as shown in Fig. 2. In principle, a mixer or a multiplier can be considered a frequency extender, but modern electromagnetic measurement requires the higher performance of extenders, the key parameters include output power, stability, and dynamic range.

There are many types of tests and measurements that require frequency extenders, such as antenna measurements, on-wafer measurements, material characterization and wireless communication.

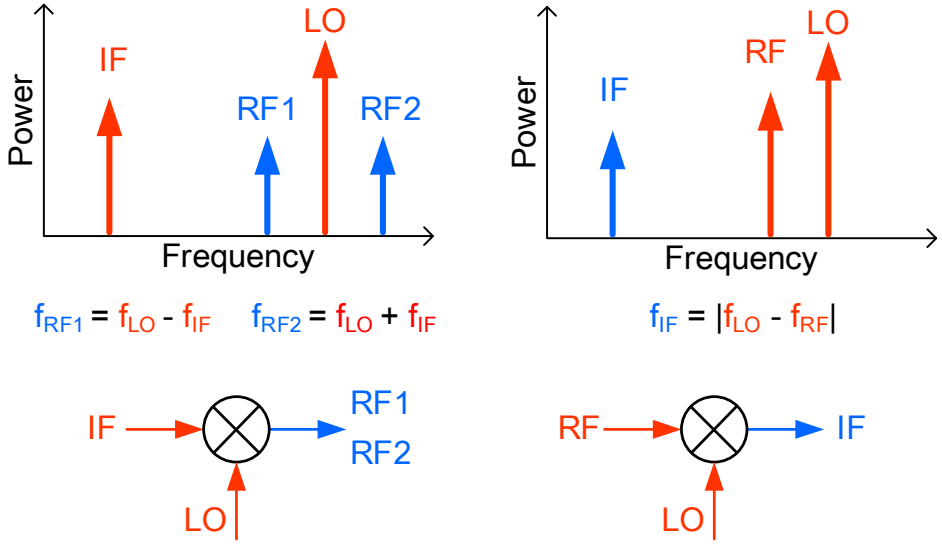

Fig. 2. Principles of (a) Frequency upconversion and (b) Frequency downconversion.

1.1 THz DFF Measurement Setup

In the DFF measurement system, the Rx side is located at the far-field (FF) distance, where the radiated electromagnetic (EM) waves from the Tx side can be regarded as plane waves. The FF distance can be calculated by using the equation of $(2D^2)/\lambda$, where D is the largest dimension of the AUT aperture size. In [8], the AUT was connected to the VNA extension module to measure the return loss $|S_{11}|$ and aligned with another module to measure the boresight gain and the FF radiation patterns. The antenna was fed through a 1-mm flange launcher (a coaxial waveguide connector). The far-field distance was short enough, and the measurement setup could be arranged in an office environment.

In [9], the THz antenna measurement setup was arranged in an anechoic chamber using a VNA and the WR-2.2 frequency extenders (325 – 500 GHz). Fig. 3 depicts the measurement setup. The alignment process includes a rough adjustment by the 3D motorized stage and a fine adjustment by the 5-axis manually moving stage. The AUT is placed at the centre of the rotary table. The IF signal is set at 1 Hz for a higher signal-to-noise ratio (SNR). The radiation pattern coverage between $\pm 90°$ is measurable, and the SLL and HPBW of the AUT are provided. The rotary table can only rotate in the horizontal plane. The Rx antenna and the AUT must rotate 90 degrees to measure another plane. When measuring the cross-polarization of the AUT, the AUT and the Rx antenna need to be placed orthogonally.

At the THz band, the measured gain curves tend to have a small fluctuation of about 0.5 dB. This is due to the following reasons: (1) The output power of the THz source is relatively weak. Finding a THz source with a stable gain and a wide frequency bandwidth is challenging. (2) During radiation pattern measurement, the vibration of the rotary table can lead to measurement uncertainty [10].

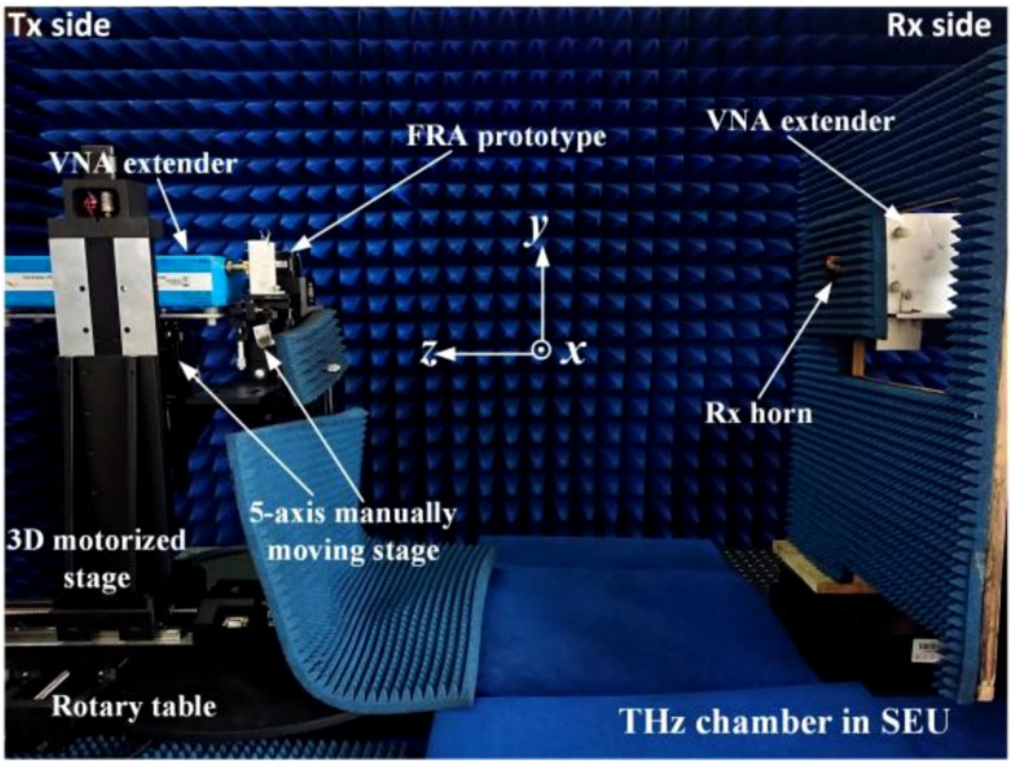

Fig. 3. Terahertz antenna measurement setup in the anechoic chamber [9].

1.2 THz IFF Measurement Setup

When testing an electrically-large antenna, the long far-field distance in DFF measurement inevitably introduces a significant atmospheric absorption. The compact antenna test range (CATR) is one type of IFF measurement that uses lenses [11] or reflectors [12] to generate a uniform plane wave, and the distance between the Tx and Rx sides can be reduced. Therefore, the IFF measurement system is more suitable for testing electrically large antennas. According to [13] and [14], a tri-reflector CATR system is designed by applying the synthesis-by-ray-tracing (SRT) and geometric optics (PO) techniques, as shown in Fig. 4. The reflectors achieve a quiet zone with a diameter of $3.5\ m$ and a high quiet zone usage of 70%. The operating frequency band is from 75 GHz to 325 GHz. Compared with the single-reflector and dual-reflector systems, the tri-reflector system has higher aperture usage and lower manufacturing costs. In addition, the tri-reflector system can be combined with the serrated edge technique for further improvement.

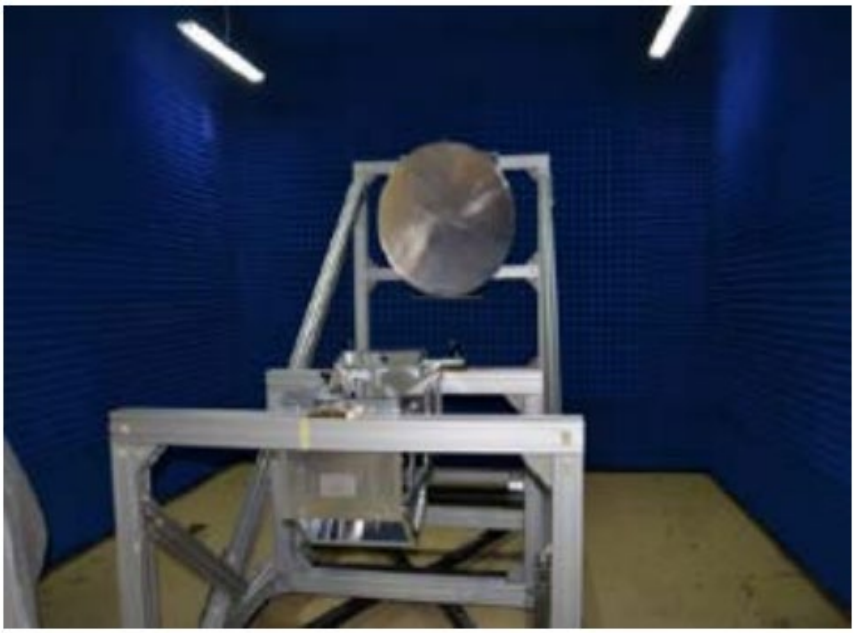

(a)

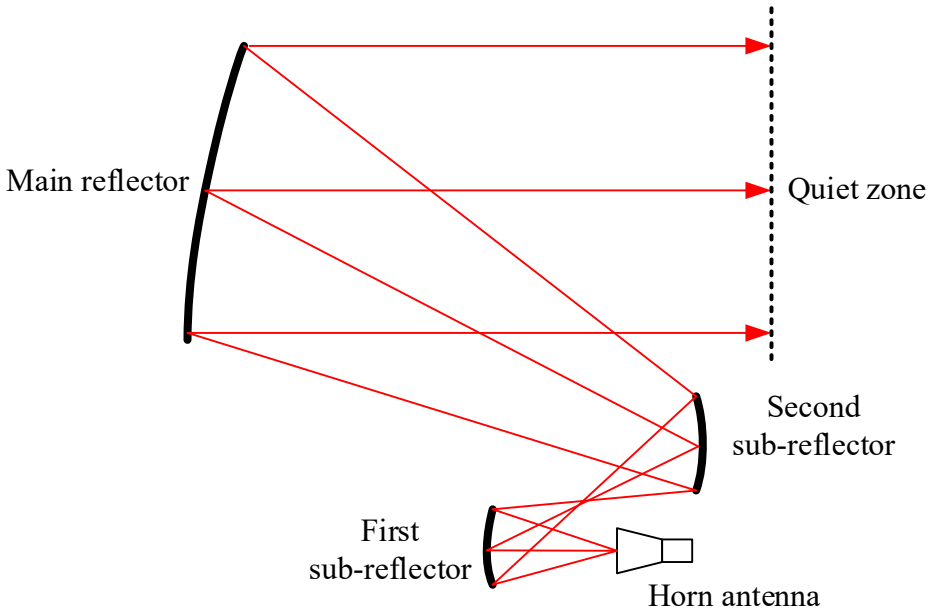

(b)

Fig. 4. (a) Photograph and configuration of tri-reflector CATR system [14]. (b) The core structure of the tri-reflector CATR system.

In [15], a CATR system based on a serrated reflector measures the boresight gain from 180 GHz to 250 GHz and the radiation pattern at the range of $\pm 50°$, as shown in Fig. 5.

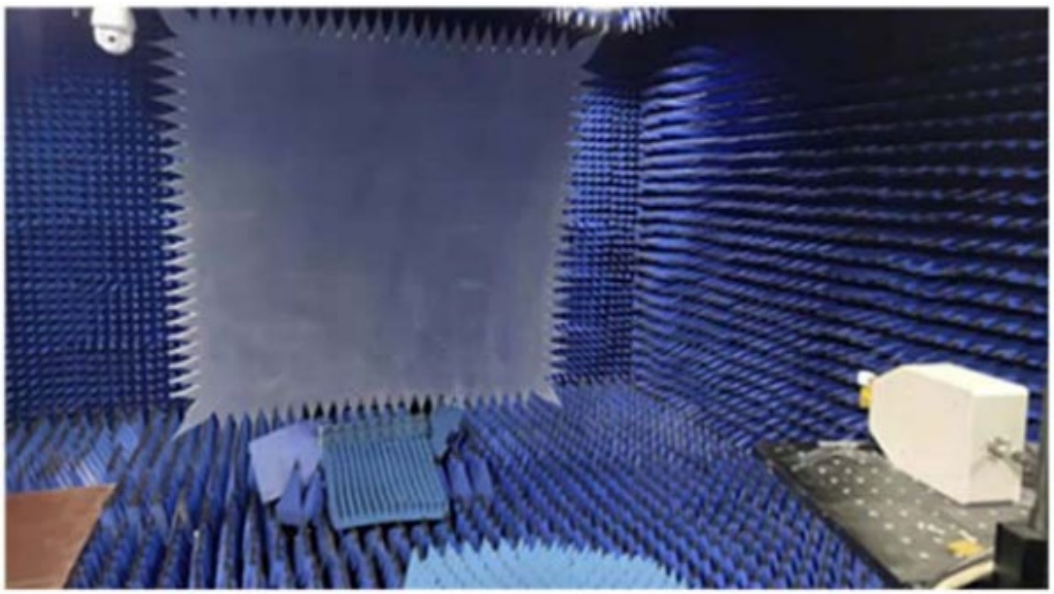

Fig. 5. Serrated edge reflector CATR measurement system [15].

1.3 THz NF Measurement Setup

In NF measurement, the far field results can be obtained by calculating the 2D Fourier transform of the NF-measured results. Depending on the scanning modes, there are three main types: planar, cylindrical, and spherical scanning [7]. In [16], a planar scanning THz NF measurement setup is proposed at 300 GHz, as shown in Fig. 6. The minimum and maximum distance between the Tx and Rx sides are $1\ mm$ and $16\ mm$, respectively. The magnitudes of the radiation fields along the propagation direction can be obtained by employing a three-axis translation stage to control the Rx side. The measurement setup is placed on an optical table to minimize the vibration, and the front surface of the frequency extenders is covered by an absorber.

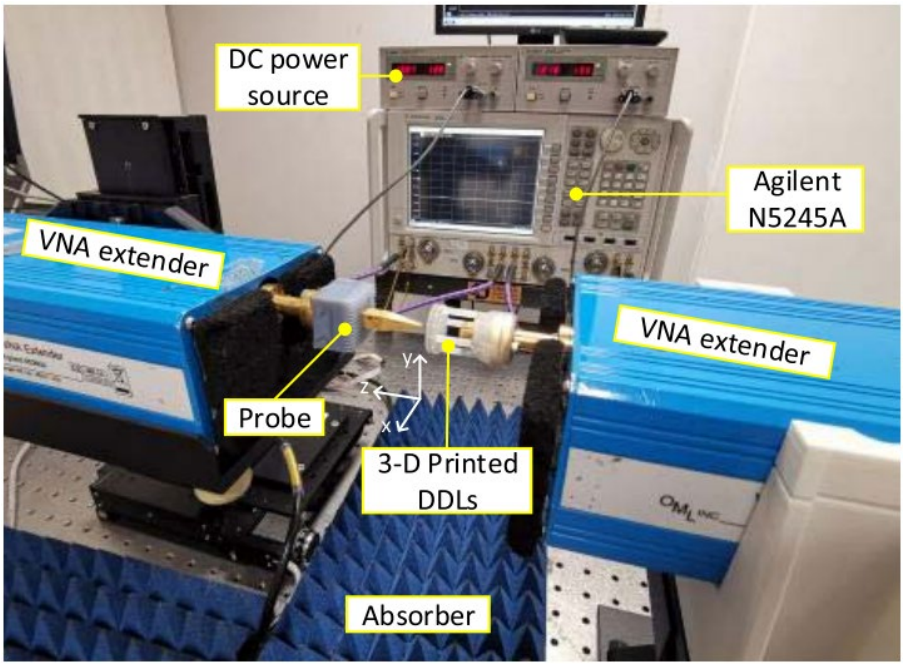

Fig. 6. Terahertz near-field measurement setup [16].

1.4 On-Wafer Measurement Setup

On-wafer measurements are widely used in chip measurement. It can be used at different stages of the chip manufacturing process, improving testing efficiency and providing more accurate measurement results. The ground-signal (GS) probes or ground-signal-ground (GSG) probes are utilized to feed the device under test (DUT). A waveguide-to-GSG probe is needed to connect with the frequency extender [17]. A wafer chunk can retain the DUT and reduce the EM reflections.

In [18], the setup for an antenna measurement between 220 GHz and 325 GHz is shown in Fig. 7. A harmonic mixer is used to downconvert the RF signal to the IF signal, and the VNA receives the IF signal. An OML T/R module was connected to a VNA (PNA-X), the coplanar probe contacted the AUT at the wafer chuck, and a horn antenna was rotated around the AUT. Therefore, the system can measure the return loss (S_{11}) and the radiation pattern of the AUT. The maximum distance between the horn antenna and the AUT is 75 cm. This limits the aperture size of the AUT.

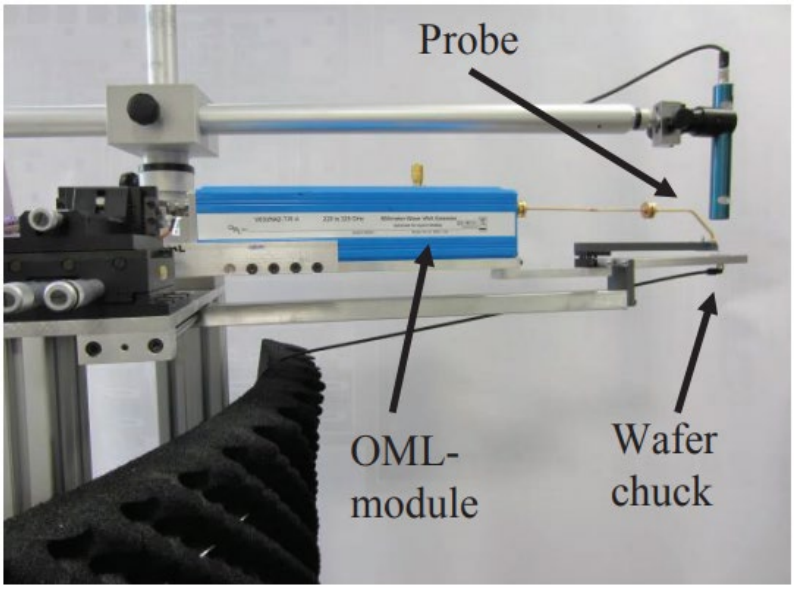

(a)

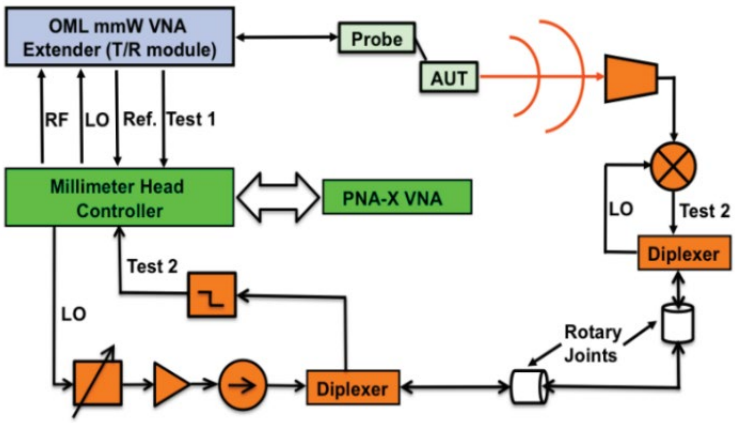

(b)

Fig. 7(a) Tx side of the on-wafer measurement setup, (b) Schematic diagram of the setup [18].

In [19], a THz antenna-on-chip (AoC) measurement setup was proposed. The

measurement setup is shown in Fig. 8. The hemispherical plastic positioning system was utilized for the far-field measurement. The rectangular frame marked with yellow-black tape is a plastic wood composite material to reduce the reflection. By comparison, a metallic positioning system will cause measurement uncertainty in radiation patterns if the absorber is not covered on the surface of the system. The rotary joint can hold the RF and DC cables to prevent the lines from getting tangled. The elevation PTFE (Polytetrafluoroethylene) hook holds the receiver. The receiver can move along the hook. Thus, a full elevation half-plane is measurable. The wafer chunk can be fixed for on-wafer probe measurements and moved away for waveguide measurements. The microscope is connected to a camera for observing the DUT. The VNA and frequency extension modules are used to measure the S-parameters ($|S_{11}|$, $|S_{12}|$) and FF radiation pattern between 220 and 330 GHz. The φ and θ polarization can be measured. Thin absorbers were applied to cover the metallic probe to suppress the radiation from the probe tips.

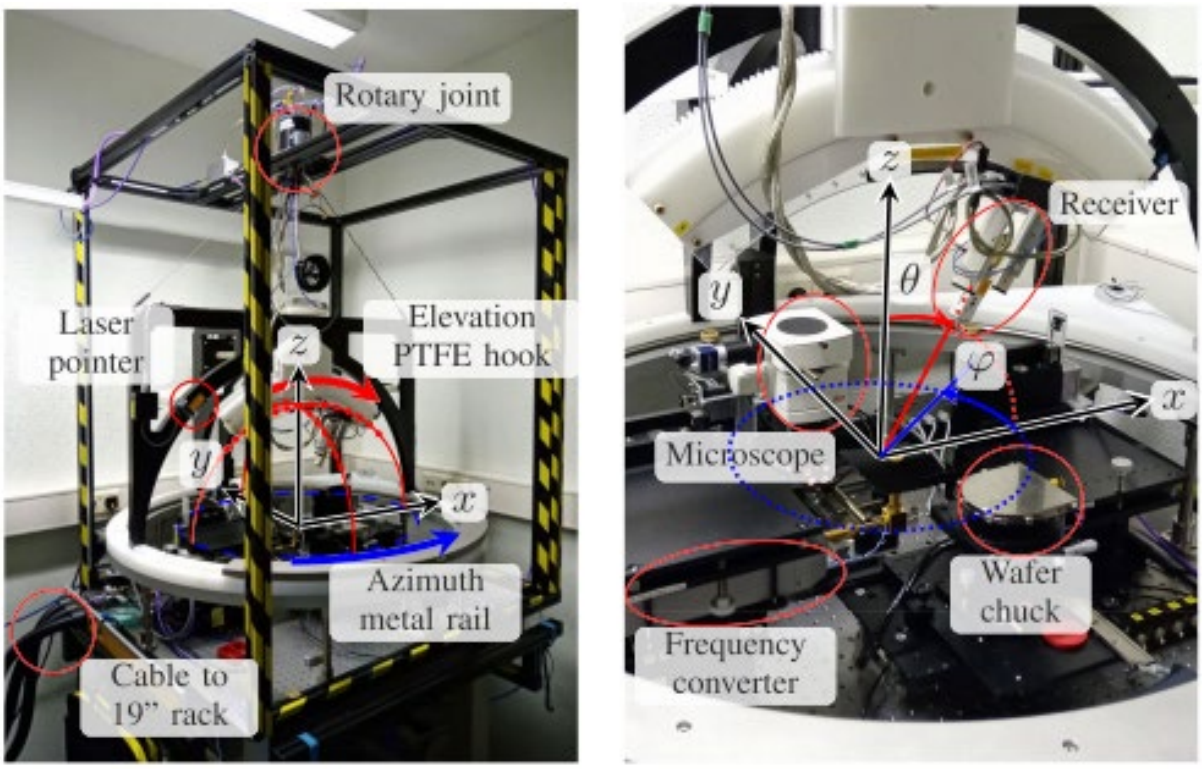

Fig. 8. Photograph of the upper hemisphere measurement setup [19].

In [20], a robotic arm is used in on-wafer measurements up to 280 GHz, as shown in Fig. 9. The robot positions the Rx side of the measurement system. The robot has six degrees of freedom with a positional precision of $350\ \mu m$. The measurement setup can realize a flexible transformation from near-field to far-field measurements. When measuring the radiation patterns, the scanning range is over $\pm 90°$ for a distance of $150\ mm$, and it turns into $\pm 60°$ for a distance of $250\ mm$. Theoretically, a robotic arm can implement any scanning mode, including planar, cylindrical, and spherical scanning.

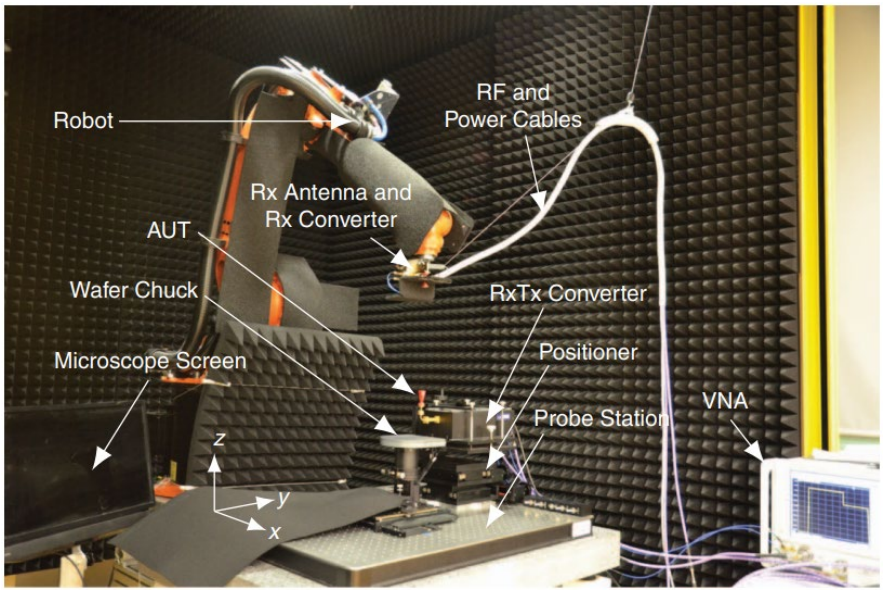

Fig. 9. On-wafer measurement by using a robotic arm [20].

Recently, THz antenna-in-package (AiP) for 6G communications has been proposed in [21]. A new probe station can provide a probe contact on the bottom of the antenna array, as shown in Fig. 10 (a). The GSG probe is upside-down, and the GSG contact pad in Fig. 10 (b) is placed at the bottom of the AiP. Additionally, Rohacel foam ($\varepsilon_r \approx 1$) is used to fabricate the AiP holder for minimum interference.

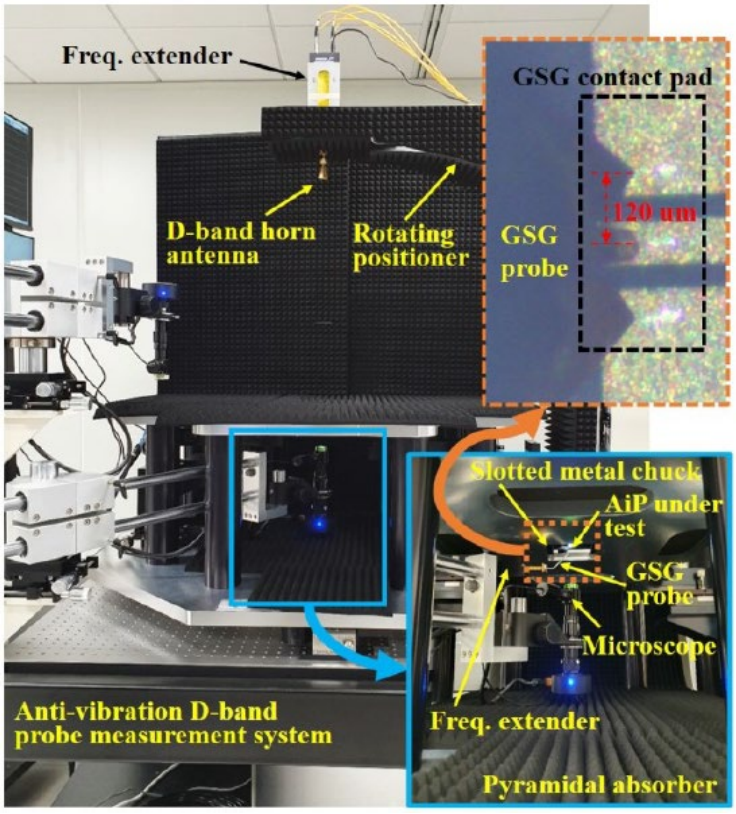

(a)

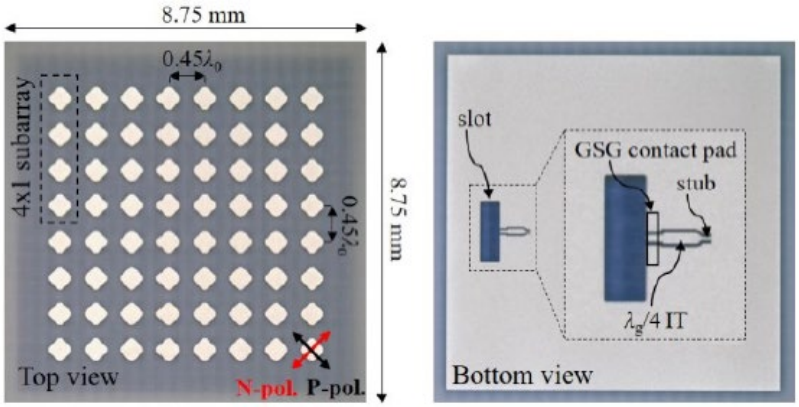

(b)

Fig. 10. (a) Photo of custom-built probe-based measurement system. (b) Top and bottom view of the AiP.

2. Photonic-Based Measurement

The basic diagram of the photonic-based measurement (PBM) systems for THz waves is shown in Fig. 11. The measurement setup consists of the laser sources, a power divider (PD), two light paths, an emitter and a detector. According to the type of laser, the PBM systems can detect the THz pulse and continuous wave (CW). The light path to the emitter can excite the THz waves using photoconductive antennas (PCAs) or optical-to-electrical (O/E) convertors, while the way to the detector is for synchronization. Because of the laser sources, the PBM systems cannot measure the reflected power of the sample under test.

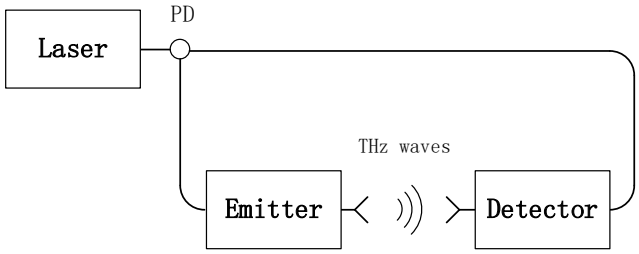

Fig. 11. The basic schematic diagram of the PBM systems

Terahertz time-domain spectroscopy (THz-TDS) [22] has become a valuable technique in various research fields, including chemistry, materials, and imaging. As shown in Fig. 12, a photoconductive antenna biased with a DC voltage can convert the laser pulse to the THz pulse. Using the pump-probe technology [23], the waveform of the THz pulse can be measured. The inverse Fourier transform converts the measured pulse into the frequency domain so that the THz frequency spectrum of about 0.1 – 3 THz is obtained. The THz-TDS system is shown in Fig.12; the whole system consists of two spatial light paths for pulse synchronization, which limits the distance between the emitter and the detector. Therefore, it is rarely used in radio frequency (RF) antenna measurements.

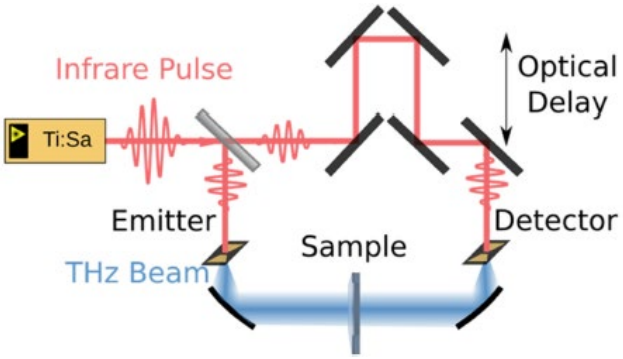

Fig. 12. Schematic of a THz-TDS setup [24]. Ti:Sa means a femtosecond Ti:Sa laser.

2.1 THz Waves Generation

The photoconductive antennas (PCAs) are commonly used in the THz-TDS systems as the key part of the emitters. However, they cannot connect to the antennas under test (AUTs). To realize O/E conversion, a uni-travelling-carrier photodiode (UTC-PD) [25,26] was applied for CW generation. As shown in Fig. 13, two laser beams with different frequencies (f_1 and f_2) combined by a coupler pass through the photodiode and generate a radio-frequency (RF) signal of $f_1 - f_2$, called "optical heterodyning" [27], which is the cost-effective and simple way to obtain the widest frequency tenability from GHz to THz. However, the frequency stability of the acquired RF signals is poor.

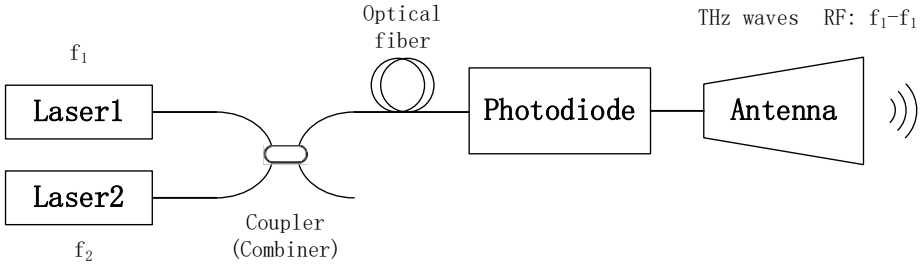

Fig. 13. THz wave generation by optical heterodyning.

2.2 THz Waves Detection

The early THz systems detect the THz waves using photoconductive switches for THz pulse measurement. In Fig. 14, the photoconductive antenna (PCA) combined with the external circuit is referred to as a "photomixer" for THz wave detection [28].

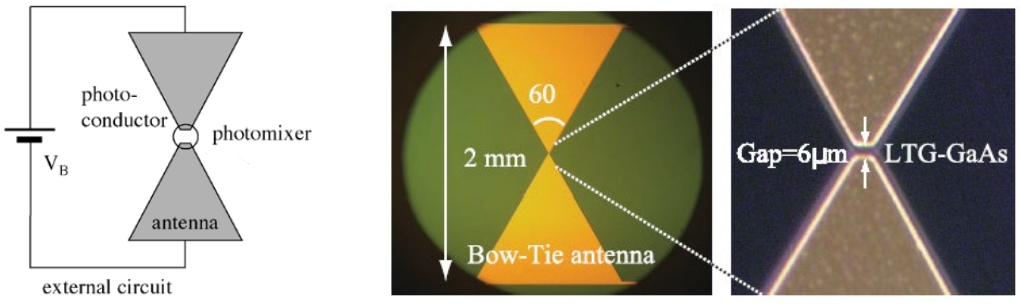

(a) (b)

Fig. 14. (a) Schematic of a photomixer for CW-THz wave generation [28]. (b) Photos of an LTG-GaAs-based photoconductive antenna [29]

In Fig. 15, the electro-optic (EO) probe consists of a high-reflection (HR) mirror, EO crystal, and gradient-index (GRIN) lens connected to the polarization-maintaining fibre (PMF). The EO probe can be divided into five types [30]. The HR mirror has a high reflection coefficient for the optical beam. It can reflect all the optical beams but cannot reflect the EM waves. The EM waves interact with the LO optical beams in the EO crystal so that the EO modulation occurs. The E-fields' amplitude and phase information are transferred to the LO optical beams because the refractive index of the EO crystal changes with the applied E-field. When measuring the E-field, the polarization of the E-field needs to be parallel to the optic axis of the EO crystal.

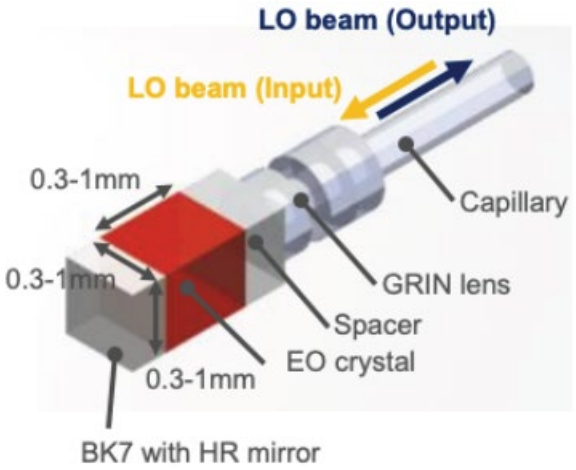

Fig. 15. Photo of the EO probe [31]

2.3 Development of the PBM Systems

In 2000, the electro-optic (EO) probe was employed to measure the NF pattern of a 4 GHz patch antenna [32]. The measurement system is based on the microwave synthesizer to generate a low-frequency signal. A photodiode is used to downconvert from the laser signal to an RF signal, and a spectrum analyzer detects the signal.

In 2017, a UTC-PD was applied for the 80 GHz continuous wave generation, and the RF signal was received by a ZnTe EO THz probe. The measurement system [25] is presented in Fig. 16. The EO detector is composed of half mirrors and a $\lambda/2$ wave plate and a $\lambda/4$ wave plate. A spectrum analyzer measured the 100 kHz signal downconverted from 80 GHz.

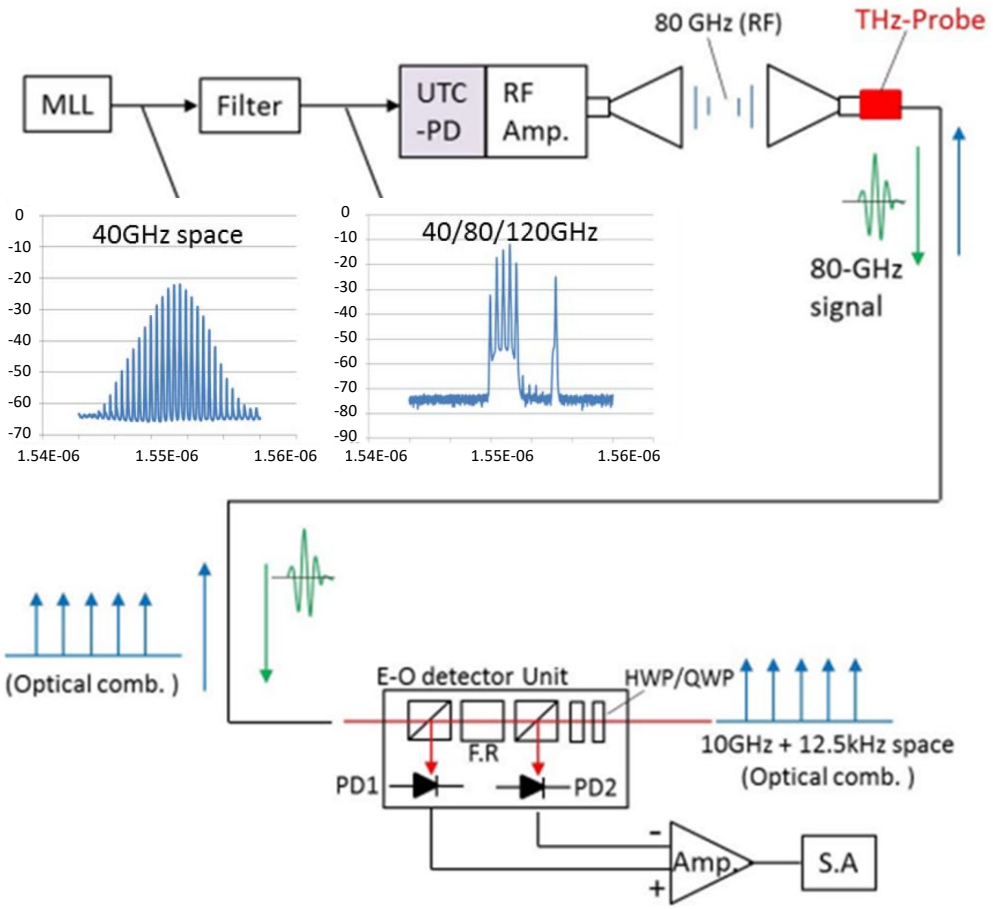

Fig. 16. Experimental setup for 80 GHz signal detection. MLL: mode-lock-laser.

In 2017, a commercial PBM system from EMAG Technologies, NeoScan, was used for 40 MHz and 4.8 GHz antenna measurement [33,34]. The system was based on the Pockels effect of the EO probe.

In 2022, the photonics technology was applied to the antenna measurement system, as shown in Fig. 17. Using a robot arm, a planar and cylindrical scanning THz NF measurement setup was proposed at Gifu University. The operating frequency band from 1 GHz to 600 GHz is achieved. The photonics technologies include the EO sensing technique [35], non-polarimetric frequency down-conversion technique [36] and self-heterodyne technique [25]. Compared with a conventional metallic probe antenna, the EO probe head is extremely small, and the aperture size of $0.2mm \times 0.2mm$ is realizable. Because the probe is made of crystal, like GaAs, and $LiTaO_3$, the influence on the field is negligible when measuring the near-field, which means low invasiveness. Then, the EO probe is extremely light, which will not introduce deflection when scanning the probe by using a robotic arm. In addition, the signal was transmitted through low-loss and flexible fibres. The scanning of the robotic arm can be flexible. Finally, the operating frequency band of the system was wider, with no need to change the EO probe.

The NF-measured amplitude and phase distribution of a rectangular horn antenna at 77 GHz agreed well with the simulated ones. The calculated radiation patterns from measured NF distribution at 286 GHz agreed well with the FF measurement by the VNA solution. The

system could not measure the return losses ($|S_{11}|$) of the AUT. The basic setup and principle of the antenna measurement system are as follows.

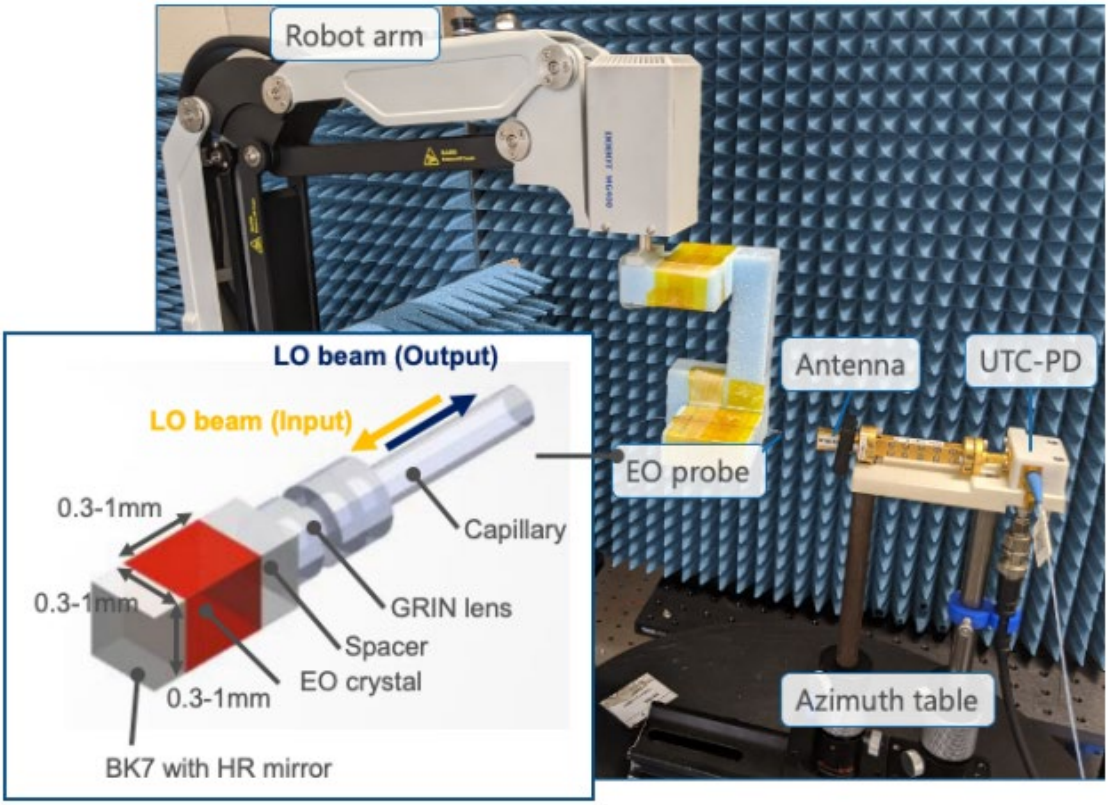

Fig. 17. EO probe with a robot arm. A WR-3.4 rectangular horn antenna is being tested. GRIN lens: graded index lens, HR mirror: high reflection mirror [31].

In Fig. 18, the non-polarimetric frequency down-conversion technique [36] employed the wavelength filter (WF) instead of the wave plate (WP). For conventional EO field detection, the dual-frequency laser source includes two lasers with different frequencies ($f_1, f_2, f_2 > f_1$) and is split by a Gipower divider (PD) into two arms. Arm 1 was used to generate an RF signal. Arm 2 was applied for transferring optical signals. The path delay difference between the two arms was minimized by adjusting the optical delay line. As shown in Fig. 18 (a), the birefringence effect of the EO crystal was utilized in conventional EO field detection. The E-field from RF signal could affect the EO crystal, and birefringence occurred. Thus, the polarization of light coming out of the EO crystal was changed. The polarization change relates to the intensity of the applied E-field [37]. Adjusting the WP allows the output light to remain unchanged or realize a 90-degree polarization rotation. The analyzer is a polarizer. Thus, the intensity of the two polarizations of the input light can be detected, and the polarization change can be deduced. Finally, the intensity of the RF signal is obtained. However, this method can only detect the intensity of the E-field.

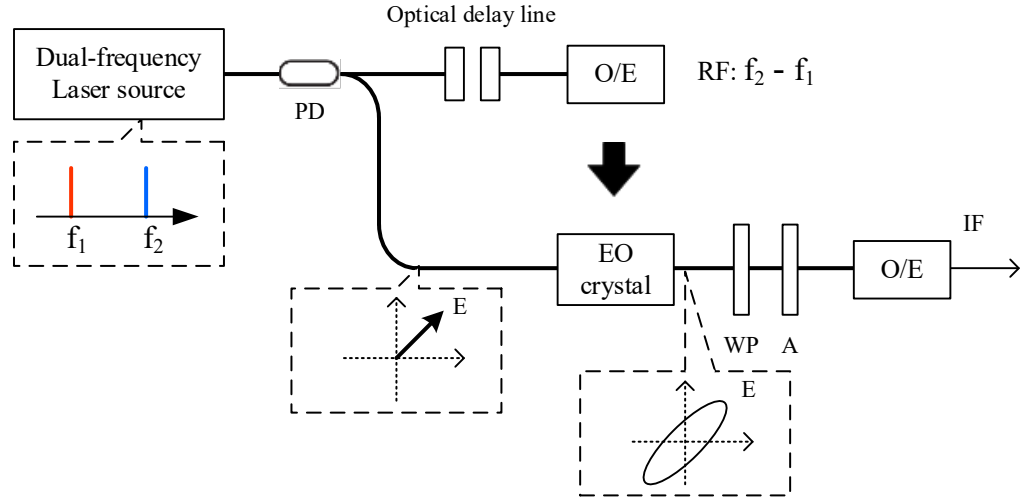

(a)

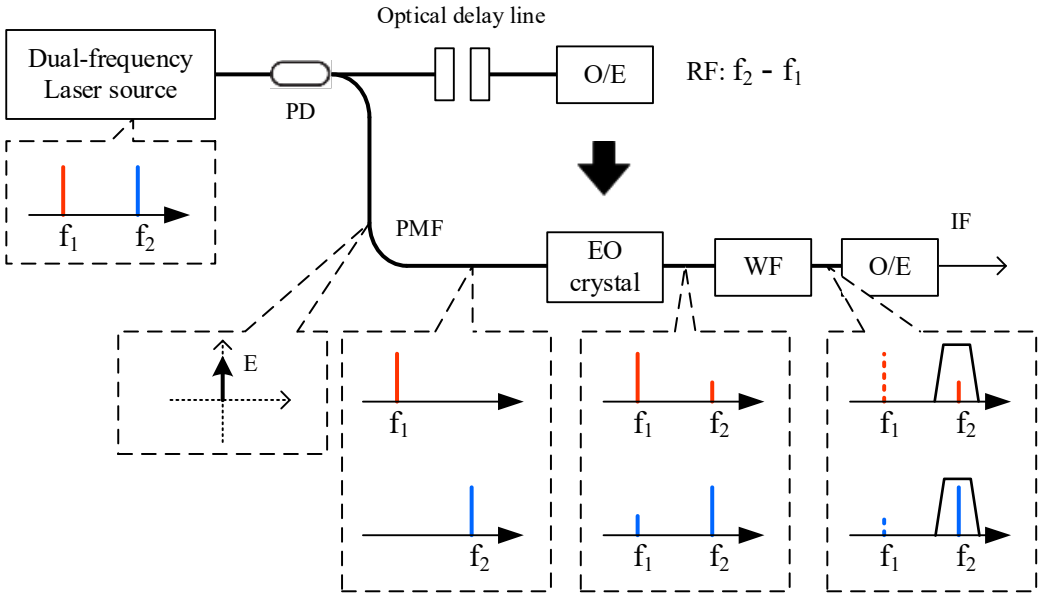

(b)

Fig. 18. Comparison between (a) Conventional and (b) Non-polarimetric homodyne-type EO field detection. PD is a power divider, O/E is an optical-to-electrical converter, WP is a wave plane, A is an analyzer, and WF is a wavelength filter. PMF: polarized, maintaining fibre.

The non-polarimetric homodyne-type EO field detection utilized the photomixing effect of the EO crystal. The RF signal interacts with two laser carrier. f_1, f_2 respectively, and generates their corresponding sidebands. In Fig. 18 (b), the upper frequency f_2 passes through the filter. In this way, this method shows a 1.5-fold increase in detection sensitivity compared to the conventional method and the information of the RF signal, including the amplitude and the phase, is transferred to the downconverted IF signal. However, in [20], the IF signal was detected by a spectrum analyzer, and the dynamic range is about 40 dB. This detection system still cannot realize the phase measurement, the precise frequency tunability and the higher frequency resolution for continuous waves (CWs). However, the CW measurement system using EO crystal began to take shape.

The self-heterodyne system [29] is a modified homodyne system. The core component is the "photomixer (PM)". Its function is similar to the aforementioned mixer in Fig. 2. As shown in Fig. 19 (a), two frequency detuned lasers ($f_1, f_2, f_2 > f_1$) are combined. The laser beam at the frequency of $f_2 - f_1$ is generated and split into the RF Arm and the LO Arm. By using an O/E converter (UTC-PDs), the frequency of the THz wave turns to $f_2 - f_1$. The THz wave is measured by a photoconductor or a photodiode, which works as a mixer. The amplitude and phase detection principle was similar to the dual-phase lock-in (DPLI) amplifier [38]. By changing the optical delay line, the phase of the RF signal can be different from that of the LO signal. The optical delay line needed to introduce two phases: in-phase ($\mathbf{0°}$) and quadrature-phase ($\mathbf{90°}$). The in-phase and quadrature-phase states induced two detected signals. The detected signals were regarded as two equations to calculate two unknown variables, the amplitude and the phase of the RF wave, and then the THz wave was detected. However, suppose the lasers occur frequency fluctuations. In that case, the frequency fluctuation would be converted into phase fluctuation because the optical delay line was related to both the path length and the frequency. This method required two stable lasers. The varying delay line is relatively slow.

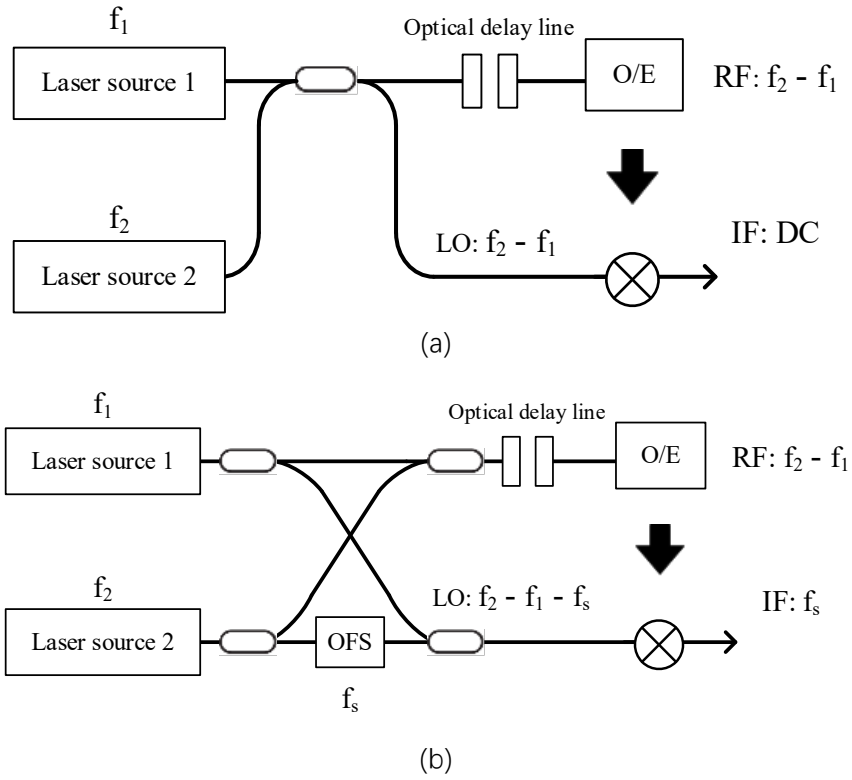

Fig. 19. Comparison between (a) Homodyne system and (b) Self-heterodyne system. OFS: optical frequency shifter.

For the self-heterodyne system in Fig. 19 (b), an optical serrodyne frequency shifter (FS) is added to introduce additional frequency f_s. The path length of the RF Arm is equal to that of the LO Arm in this case. The IF signal contained the RF signal information, while the RF Arm's phase noise was cancelled with the LO Arm. By using DPLI detection, the amplitude and phase of the IF signal can be obtained. The f_s frequency source can be used as the reference signal for DPLI detection. In [29], a 300 GHz THz wave was generated by using a J-

band UTC-PD with an output power of 30 μW, and the frequency f_s was set as 2 kHz. A photoconductive antenna (PCA) was used as a mixer to receive the RF and optical LO signals and generate the IF signal. The photoresponse between the received LO signal and the output IF signal was linear. The IF signal range was from -90 dB to -60 dB. The amplitude fluctuation is $\pm 2.7\%$. In [39, 40], the photonic-based measurement systems based on the self-heterodyne system were mature, so the basic setup did not change much. In Fig. 20 (a), the orange lines represent the optical fibres, while the blue lines are electrical cables. The frequency of the THz wave is $f_2 - f_1 - f_s$. The EO frequency shifter (FS) introduces the frequency f_s of 100 kHz – 10 MHz, which allows electric phase synchronization between the generation and the detection. Thus, precise phase measurement can be achieved. The EO probe is used as a mixer and connected to a circulator. The LO optical signal goes through the circulator to the EO probe and interacts with the RF signal in the EO crystal. Then, the generated IF signal is transmitted to the optical band pass filter (OBPF) through the circulator. The photograph of the photonic-based measurement system is shown in Fig. 20 (b). The distance between the EO probe and the AUT is set as 2mm. The EO probe scans the cut section of the AUT with an area of 11 mm × 13 mm, and the scanning step is 0.1 mm. The EO probe has a cross-polarization suppression ratio of 22 dB. Using the 2D Fourier transform, the NF-measured result can be transformed into the 3D far-field radiation pattern.

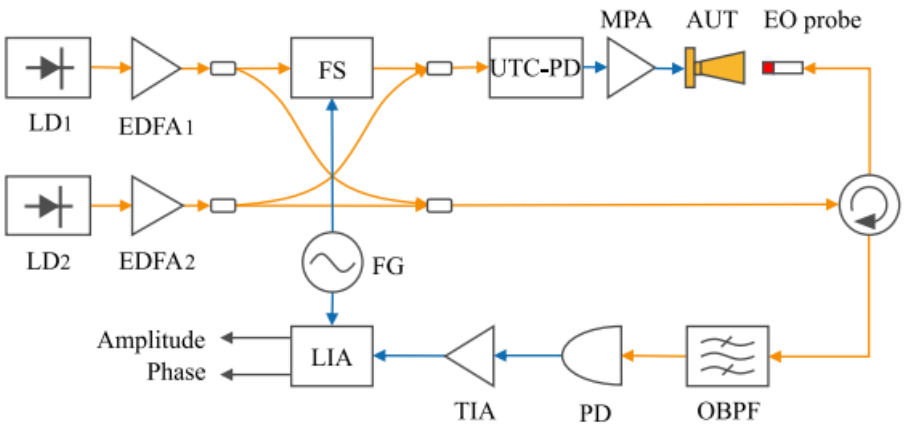

(a)

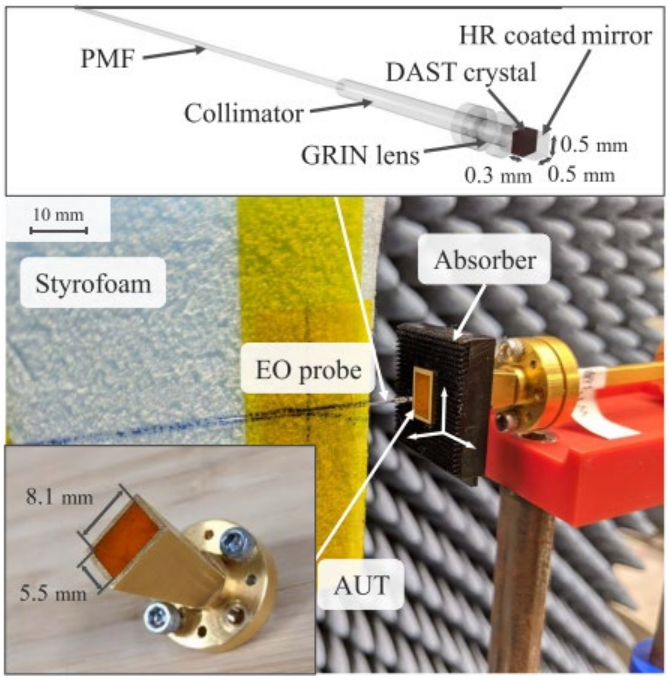

(b)

Fig. 20. (a) Schematic diagram of the measurement setup. m. LD: laser diode; EDFA: erbium-doped optical amplifier; MPA: medium power amplifier; OBPF: optical bandpass filter; PD: photodiode; TIA: transimpedance amplifier; and LIA: lock-in amplifier. (b) Photograph of the measurement setup [40].

3. Comparison Between The Solid-State Electronics-Based and Photonic-Based Measurement

The difference between the two methods is the THz wave generation and detection methods. Although the operating frequency still needs to be increased, the solid-state electronics-based measurement (SSEBM) systems are relatively mature technologies and can provide customized specifications based on practical needs. On the other hand, photonic-based measurement (PBM) systems are the newly developed technologies. However, the PBM systems have additional advantages: (1) The detection probe is small and made of dielectric materials, which makes it suitable for NF measurement without field disturbance. (2) Compared with the frequency extenders, the detection probe is extremely light, which has little effect on the movement of the scanner. (3) The PBM systems utilize fibres to transmit signals, which has more advantages than RF cables, including loss, flexibility, and longer line length. (4) The operating frequency band of the PBM systems can reach from 1 GHz to 600 GHz [31].

3.1 Comparison Between Simulation and Measurement

As for the solid-state electronics-based measurements (SSEBMs), the results of the radiation patterns at 240 GHz [18] in 2013 are shown in Fig. 21. The ripples are severe, and the radiation of the GSG probe affects the measured results in the $280°$ direction of the E-plane. To resolve the influence of the probe, the GSG probe in [41] is placed under the

antenna, and the comparison results are shown in Fig. 22. Three antenna samples are measured to verify the fabrication tolerance. The sidelobes of the simulated and measured radiation pattern match better in the range of $\pm 60°$.

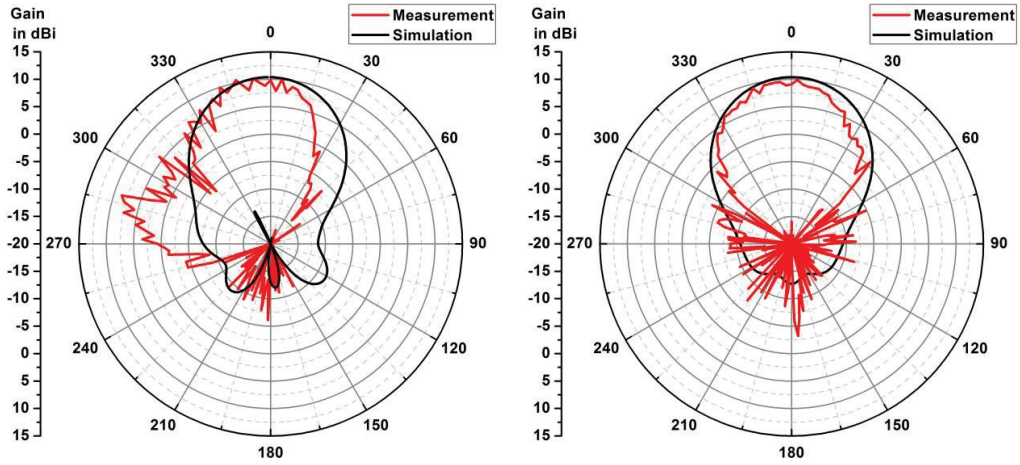

Fig. 21. Simulation results of the radiation pattern at 240 GHz compared with measurements using the SSEBM method [18]; (a) E-plane; (b) H-plane.

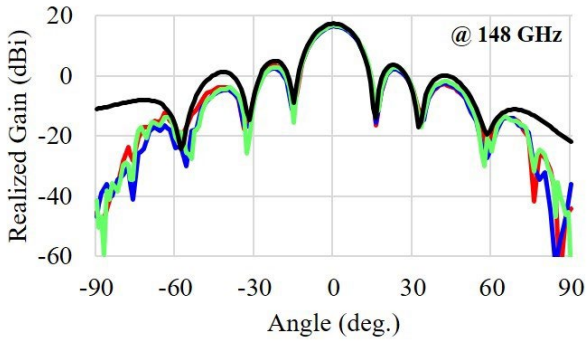

Fig. 22. Simulation results of the radiation pattern at 142 GHz compared with measurements using the SSEBM method [41].

In recent years, the SSEBM has been applied for the THz antenna measurement above 300 GHz. As presented in [9], using direct far-field (DFF) measurement setups, the WR-2.2 horn antennas were used to measure radiation patterns at 400 GHz in the THz anechoic chamber. The comparison between simulated and measured Co-polarized radiation patterns in Fig.23 has a good agreement in the range of $\pm 30°$; there are minor ripples in other ranges, but the overall trend is relatively close. Using IFF measurement setups, good agreement in [14] still exists within $\pm 30°$. The solid-state electronics-based measurements (SSEBMs) can maintain good agreement between simulation and measurement within the normalized range of at least -30 dB.

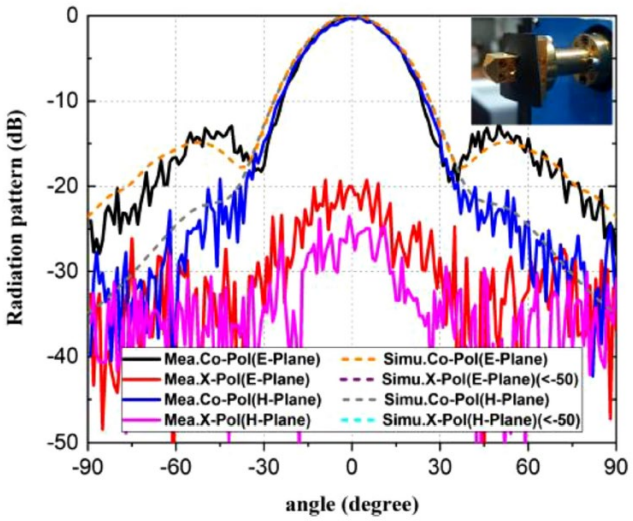

Fig. 23. Simulation results of the radiation patterns at 400 GHz compared with measurements using the SSEBM method [9]

The comparison between the photonic-based and conventional measurement systems [40] is shown in Fig. 24. The antenna under test is a pyramid WR-3.4 horn antenna, and both measurement results are almost consistent within the normalized range of -30 dB.

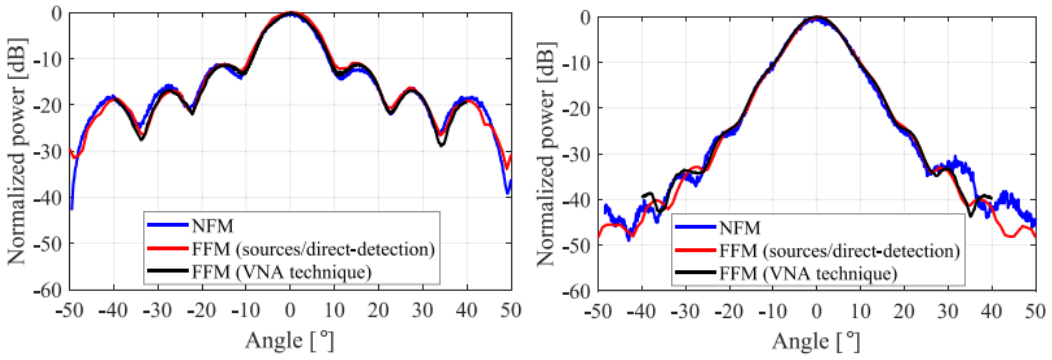

(a) (b)

Fig. 24. Comparison of the radiation patterns at 300 GHz between the photonic-based and conventional measurement systems (solid-state electronics-based solution) at (a) E-plane and (b) H-plane. NFM: near-field measurement from the PBM system. FFM: far-field measurement [40].

3.2 SSEBM and PBM Performance Comparison

Table 1 lists the parameters and capabilities of the solid-state electronics-based measurement (SSEBM) and photonic-based (PBM) setup for comparison. The frequency of the SSEBM systems comes from the frequency extenders. More detailed information can be found from the manufacturer. For the SSEBM systems, the feed interfaces of almost all the frequency extenders are waveguides, while the PBM systems use the UTC-PD to feed a waveguide antenna. The GSG probe is linked to a waveguide through a converter in the THz band; thus, this case counts as a waveguide feed. The UTC-PD has the output power of -14 dBm at 286 GHz [38], and the radiated power of the THz wave in [37] was 650 μW (about -1.87 dBm) at 125 GHz, which contains the gain of a horn antenna. By comparison, according

to data from the VDI Mini extension modules, the typical test port output power was 18 dBm in the frequency band of 110 - 170 GHz, while output power in the frequency range from 220 to 330 GHz was 6 dBm. Regarding the radiated power, the PBM system has the potential to realize the DFF and IFF tests. The PBM systems utilize fibres to transmit signals, which has more advantages than RF cables, including loss, flexibility, and line length. Dynamic range is the ratio between the largest and smallest values that a certain power can be detected, which is an essential performance for antenna measurement systems. As for the SSEBMs, a probe-based millimeter-wave antenna measurement system [42] has a dynamic range of more than 60 dB at 50 to 110 GHz. The dynamic ranges for return and insertion losses are better than 20 and 35 dB at 325 to 508 GHz [5], and the dynamic ranges of the frequency extender [7] reach 60 to 80 dB from 1.1 THz to 1.5 THz. On the other hand, the electro-optic (EO) probe in [30] is expected to have a 120 dB dynamic range, while the PBM system in [36] has a dynamic range of about 40 dB.

TABLE 1. A COMPARISON BETWEEN SSEBM AND PBM

	SSE-based Measurement	Photonic-based Measurement
Frequency (GHz)	110-170 170-260 260-400 330-500 500-750 750-1100	1-600
Feed Interfaces	Waveguide fed	Waveguide fed
DFF Test	√	×
IFF Test	√	×
NF Test	√	√
3D Radiation Pattern	√	√
Gain Measurement	√	√
Return Loss Measurement	√	×
Amplitude Measurement	√	√
Phase Measurement	√	√
D-band Output Power	18 dBm	-
J-band Output Power	6 dBm	-14 dBm
Dynamic range	60 dB	40 dB
Scanning Range	±90°	±50°
Transmission Line	RF cables	Fibers
Cost	High	Moderate
Reference	[8-20]	[29,31,39,40]

3.3 Atmospheric Absorption Challenges

There are several methods to tackle the atmospheric absorption challenges. The Compact Antenna Test Ranges (CATRs) is one type of IFF measurement that uses lenses [11]. To overcome the atmospheric absorption at millimeter-wave for 5G, Keysight and Anritsu proposed CATR anechoic chamber as a measurement solution to satisfy the conformance testing of the 3GPP standards, which can give a hint to THz antenna measurement systems. Because the distance between the transmitter and receiver is reduced, the atmospheric absorption in the CATR can be negligible. As shown in Fig. 25, due to the minimal impact of the electro-optic (EO) probe on the electric field [40], the distance between the EO probe and the AUT can be set as 2 mm for near-field (NF) measurement. According to the measurement procedure, the 2D NF distribution can be obtained, and the far-field radiation pattern can be calculated using the 2D Fourier transform from the measured NF distribution. The distance between the EO-probe and the antenna under test is only 2 mm. Thus, the atmospheric absorption is negligible.

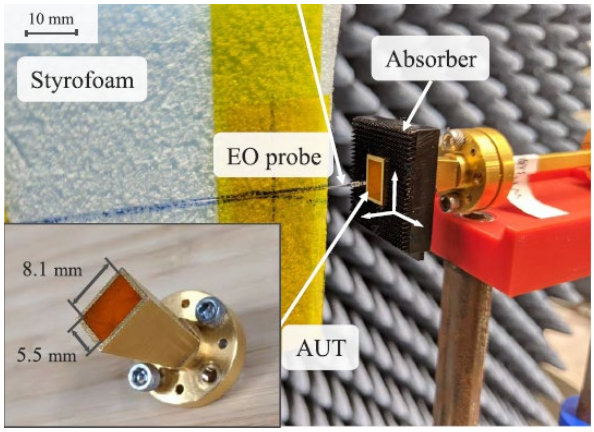

Fig. 25. Photo of the PBM IFF measurement setup [40].

In recent years, transmitarray antennas (TAAs) [9] have received much interest in the THz frequency band due to their ease of fabrication and measurement. Their high-gain performance can overcome atmospheric absorption, making TAAs suitable for DFF Measurement Setups.

4. Conclusion

This article comprehensively reviewed and compared the solid-state electronic-based and photonic-based terahertz antenna measurement systems. The classification of the two systems (SSEBMs and PBMs) is based on THz wave generation and detection principles. The SSEBM systems included direct far-field (DFF), indirect far-field (IFF), near-field (NF), and midfield measurement setups, and the PBM systems also have the potential to develop into these modes. Terahertz antenna measurement requires customized specifications based on case-by-case applications. The discussions in this article provide the basic references for building a THz antenna measurement platform.

Reference

[1] I. R. R. Barani, L. A. Bronckers and A. C. F. Reniers, "Integrated-Antenna Over-the-Air Testing for Millimeter-Wave Applications: An Overview of Systems and Uncertainty [Measurements Corner]," in *IEEE Antennas and Propagation Magazine*, vol. 64, no. 5, pp. 97-110, Oct. 2022.

[2] D. Rytting, "ARFTG 50 year network analyzer history," *2008 71st ARFTG Microwave Measurement Conference*, Atlanta, GA, USA, 2008, pp. 1-8.

[3] T. Gaier, L. Samoska, C. Oleson, and G. Boll, "On-wafer testing of circuits through 220 GHz," in *Ultrafast Electronics and Optoelectronics,* Snowmass, CO, Apr. 1999, pp. 20–26.

[4] A. K. Fung, D. Dawson, L. Samoska, K. Lee, C. Oleson and G. Boll, "On-Wafer Vector Network Analyzer Measurements in the 220-325 GHz Frequency Band," *2006 IEEE MTT-S International Microwave Symposium Digest*, San Francisco, CA, USA, 2006, pp. 1931-1934.

[5] A. Fung et al., "Two-Port Vector Network Analyzer Measurements Up to 508 GHz," in *IEEE Transactions on Instrumentation and Measurement*, vol. 57, no. 6, pp. 1166-1170, June 2008.

[6] T. W. Crowe, B. Foley, S. Durant, K. Hui, Y. Duan and J. L. Hesler, "VNA frequency extenders to 1.1 THz," *2011 International Conference on Infrared, Millimeter, and Terahertz Waves*, Houston, TX, USA, 2011, pp. 1-1.

[7] D. Koller, S. Durant, C. Rowland, E. Bryerton and J. Hesler, "Initial measurements with WM164 (1.1–1.5THz) VNA extenders," *2016 41st International Conference on Infrared, Millimeter, and Terahertz waves (IRMMW-THz)*, Copenhagen, Denmark, 2016, pp. 1-2.

[8] M. S. Rabbani and H. Ghafouri-Shiraz, "Liquid Crystalline Polymer Substrate-Based THz Microstrip Antenna Arrays for Medical Applications," in *IEEE Antennas and Wireless Propagation Letters*, vol. 16, pp. 1533-1536, 2017.

[9] Z. -W. Miao, Z. -C. Hao, Y. Wang, B. -B. Jin, J. -B. Wu and W. Hong, "A 400-GHz High-Gain Quartz-Based Single Layered Folded Reflectarray Antenna for Terahertz Applications," in *IEEE Transactions on Terahertz Science and Technology*, vol. 9, no. 1, pp. 78-88, Jan. 2019.

[10] Y. -W. Wu, Z. -C. Hao, Z. -W. Miao, W. Hong and J. -S. Hong, "A 140 GHz High-Efficiency Slotted Waveguide Antenna Using a Low-Loss Feeding Network," in *IEEE Antennas and Wireless Propagation Letters*, vol. 19, no. 1, pp. 94-98, Jan. 2020.

[11] M. Multari et al., "77 GHz Stepped Lens With Sectorial Radiation Pattern as Primary Feed of a Lens Based CATR," in *IEEE Transactions on Antennas and Propagation*, vol. 58, no. 1, pp. 207-211, Jan. 2010.

[12] A. Karttunen et al., "Antenna Tests With a Hologram-Based CATR at 650 GHz," in *IEEE Transactions on Antennas and Propagation*, vol. 57, no. 3, pp. 711-720, Mar. 2009.

[13] Xiaodong Chen et al., "A tri-reflector compact antenna test range operating in the THz range," *2015 9th European Conference on Antennas and Propagation (EuCAP)*, Lisbon, Portugal, 2015, pp. 1-3.

[14] J. Yu, H. Yu, T. Chen, J. Wang, Y. Yao and X. Chen, "Application of Compact Antenna Test Range in Terahertz Antenna Measurement," *2020 Cross Strait Radio Science & Wireless Technology Conference (CSRSWTC)*, Fuzhou, China, 2020, pp. 1-3.

[15] P. Wu, K. Liu and Z. Yu, "220 GHz High-Gain Substrate Integrated Antennas With Low Fabrication Cost Based on Higher Order Mode and PCB Technology," in *IEEE Transactions on Antennas and Propagation*, vol. 71, no. 1, pp. 18-28, Jan. 2023.

[16] G. -B. Wu, K. F. Chan, S. -W. Qu and C. H. Chan, "A 2-D Beam-Scanning Bessel Launcher for Terahertz Applications," in *IEEE Transactions on Antennas and Propagation*, vol. 68, no. 8, pp. 5893-5903, Aug. 2020.

[17] D. Hou, Y. -Z. Xiong, W. -L. Goh, S. Hu, W. Hong and M. Madihian, "130-GHz On-Chip

Meander Slot Antennas With Stacked Dielectric Resonators in Standard CMOS Technology," in *IEEE Transactions on Antennas and Propagation*, vol. 60, no. 9, pp. 4102-4109, Sept. 2012.
[18] H. Gulan et al., "Probe based antenna measurements up to 325 GHz for upcoming millimeter-wave applications," *2013 International Workshop on Antenna Technology (iWAT)*, Karlsruhe, Germany, 2013, pp. 228-231.
[19] B. Sievert, J. T. Svejda, D. Erni and A. Rennings, "Spherical mm-Wave/THz Antenna Measurement System," in *IEEE Access*, vol. 8, pp. 89680-89691, 2020.
[20] L. Boehm, F. Boegelsack, M. Hitzler and C. Waldschmidt, "The Challenges of Measuring Integrated Antennas at Millimeter-Wave Frequencies [Measurements Corner]," in *IEEE Antennas and Propagation Magazine*, vol. 59, no. 4, pp. 84-92, Aug. 2017.
[21] D. Jung et al., "Terahertz Antenna-in-Package Design and Measurement for 6G Communications System," in *IEEE Transactions on Antennas and Propagation*, EarlyAccess.
[22] J. Neu, C A. Schmuttenmaer, "Tutorial: An introduction to terahertz time domain spectroscopy (THz-TDS)," in *Journal of Applied Physics*, vol. 124, no.23, pp. 231101, Dec. 2018.
[23] L. Angrisani, G. Cavallo, A. Liccardo, et al, "THz measurement systems," in *New trends and developments in metrology*, pp. 21-48, Dec. 2016
[24] R. Peretti et al., "THz-TDS Time-Trace Analysis for the Extraction of Material and Metamaterial Parameters," in *IEEE Transactions on Terahertz Science and Technology*, vol. 9, no. 2, pp. 136-149, March 2019
[25] T. Umezawa et al., "80-GHz signal detection in high speed UTC-PD using EO sampling THz probe," *2017 42nd International Conference on Infrared, Millimeter, and Terahertz Waves (IRMMW-THz)*, Cancun, Mexico, 2017, pp. 1-2
[26] T. Umezawa et al., "Bias-Free Operational UTC-PD above 110 GHz and Its Application to High Baud Rate Fixed-Fiber Communication and W-Band Photonic Wireless Communication," in *Journal of Lightwave Technology*, vol. 34, no. 13, pp. 3138-3147, July 2016
[27] T. Nagatsuma, H. Ito, and T. Ishibashi, "High-power RF photodiodes and their applications," in *Laser & Photonics Reviews*, vol. 3, no. 1–2, pp. 123–137, Feb. 2009.
[28] I. S. Gregory et al., "Optimization of photomixers and antennas for continuous-wave terahertz emission," in *IEEE Journal of Quantum Electronics*, vol. 41, no. 5, pp. 717-728, May 2005, doi: 10.1109/JQE.2005.844471.
[29] S. Hisatake, G. Kitahara, K. Ajito, Y. Fukada, N. Yoshimoto and T. Nagatsuma, "Phase-Sensitive Terahertz Self-Heterodyne System Based on Photodiode and Low-Temperature-Grown GaAs Photoconductor at 1.55 μm ," in *IEEE Sensors Journal*, vol. 13, no. 1, pp. 31-36, Jan. 2013.
[30] D. J. Lee, N. W. Kang, J. H. Choi, et al, "Recent advances in the design of electro-optic sensors for minimally destructive microwave field probing," in *Sensors*, vol. 11, no. 1, pp. 806-824, Jan. 2011.
[31] S. Hisatake, "Near-field measurement and far-field characterization of antennas in microwave, millimeter-wave and THz wave band based on photonics," *2022 International Symposium on Antennas and Propagation (ISAP)*, Sydney, Australia, 2022, pp. 351-352
[32] Kyoung Yang, G. David, Jong-Gwan Yook, I. Papapolymerou, L. P. B. Katehi and J. F. Whitaker, "Electrooptic mapping and finite-element modeling of the near-field pattern of a microstrip patch antenna," in *IEEE Transactions on Microwave Theory and Techniques*, vol. 48, no. 2, pp. 288-294, Feb. 2000
[33] K. Sarabandi, J. Choi, A. Sabet and K. Sabet, "Pattern and Gain Characterization Using Nonintrusive Very-Near-Field Electro-Optical Measurements Over Arbitrary Closed

Surfaces," in *IEEE Transactions on Antennas and Propagation*, vol. 65, no. 2, pp. 489-497, Feb. 2017
[34] K. Sabet, R. Darragh, A. Sabet, K. Sarabandi and L. P. B. Katehi, "Using electro-optic field mapping for design of dual-band circularly polarized active phased arrays," *2017 IEEE 18th Wireless and Microwave Technology Conference (WAMICON)*, Cocoa Beach, FL, USA, 2017, pp. 1-5
[35] D. J. Lee, J. Y. Kwon, N. W. Kang, "Field analysis of electro-optic probes for minimally invasive microwave sampling," in *Optics Express*, vol. 22, no.3, pp. 2897-2909, Feb. 2014.
[36] S. Hisatake, T. Nagatsuma, "Nonpolarimetric technique for homodyne-type electrooptic field detection," in *Applied Physics Express*, vol. 5, no. 1, pp.012701, Dec. 2011.
[37] H. Togo, N. Kukutsu, N. Shimizu, et al, "Sensitivity-stabilized fiber-mounted electrooptic probe for electric field mapping ," in *Journal of Lightwave Technology*, vol. 26, no. 15, pp. 2700-2705, Aug. 2008.
[38] Chao Qi, Yiyi Huang, Wensheng Zhang, Di Zhou, Yanmin Wang and Min Zhu, "Design of dual-phase lock-in amplifier used for weak signal detection," *IECON 2016 - 42nd Annual Conference of the IEEE Industrial Electronics Society*, Florence, Italy, 2016, pp. 883-888.
[39] S. Hisatake, H. H. N. Pham, T. Nagatsuma, "Visualization of the spatial–temporal evolution of continuous electromagnetic waves in the terahertz range based on photonics technology," in *Optica*, vol. 1, no. 6, pp. 365-371, Dec. 2014.
[40] Y. Tanaka et al., "Photonics-Based Near-Field Measurement and Far-Field Characterization for 300-GHz Band Antenna Testing," in *IEEE Open Journal of Antennas and Propagation*, vol. 3, pp. 24-31, 2022.
[41] D. Jung et al., "Terahertz Antenna-in-Package Design and Measurement for 6G Communications System," in *IEEE Transactions on Antennas and Propagation*, EarlyAccess.
[42] Z. Zheng, Y. Zhang, L. Shi, L. Wu and J. -F. Mao, "An Overview of Probe-Based Millimeter-Wave/Terahertz Far-Field Antenna Measurement Setups [Measurements Corner]," in *IEEE Antennas and Propagation Magazine*, vol. 63, no. 2, pp. 63-118, April 2021.